Anisotropic electronic conduction in metal nanofilms grown on a one-dimensional surface superstructure

Naoka Nagamura,[1,*] Rei Hobara,[1] Tomoya Uetake,[1] Toru Hirahara,[1] Manami Ogawa,[2] Taichi Okuda,[2] Ke He,[2] P. Moras,[3] P. M. Sheverdyaeva,[3] C. Carbone,[3] Katsuyoshi Kobayashi,[4] Iwao Matsuda,[2] and Shuji Hasegawa[1]

[1]*Department of Physics, School of Science, University of Tokyo, 7-3-1 Hongo, Bunkyo-ku, Tokyo 113-0033, Japan*

[2]*Institute for Solid State Physics, University of Tokyo, Kashiwanoha 5-1-5, Chiba 277-8581, Japan*

[3]*Istituto di Struttura della Materia, Consiglio Nazionale delle Ricerche, Trieste, Italy*

[4]*Department of Physics, Faculty of Science, Ochanomizu University, 2-1-1 Otsuka, Bunkyo-ku, Tokyo 112-8610, Japan*

(Received 27 September 2012; revised manuscript received 2 February 2014; published 12 March 2014)

We performed *in situ* conductivity measurements by multiple microscopic probes of Ag nanofilms grown on a periodic array of indium atomic wires on Si(111). Within the investigated thickness range the transport properties differ markedly from the bulk case. The ratio between the in-plane conductivity along and perpendicular to the In wires is 1.4 for the 3 monolayer (0.7 nm) thick Ag film and approaches unity with increasing film thickness. The observed anisotropy at the initial stage of the film growth is far larger than expected from the quasi-one-dimensional quantum well electronic structure of the films and ascribed to the carrier scattering at the film/vacuum and film/substrate interfaces. Our findings show that an ordered monolayer inserted at the interface enables drastic changes of the transport behavior of the whole metal nanofilm.

DOI: 10.1103/PhysRevB.89.125415 PACS number(s): 73.21.Hb, 68.65.Fg, 73.63.Hs, 79.60.Dp

Ultrathin metal films with quantized electronic states, induced by the electron confinement along the surface normal, show intriguing electronic, spintronics, and chemical properties and novel functional behaviors [1–4] that attract both academic and technological interest. One of the most relevant examples in this context is the interlayer exchange coupling, which gives rise to the giant magnetoresistance effect in magnetic layers separated by a nonmagnetic spacer [5]. The distribution of the quantized states in the energy-momentum space is defined not only by the bulk electronic structure of the material, but also by the film boundary conditions [6]. This issue is particularly important in the nanometer thickness range, since the surface and interface layers, i.e., the film boundaries, represent a large fraction of the film structure. Chemical or morphological modifications of the surface and interface can influence deeply the properties of the whole film.

In this paper we investigate the combined effects of size quantization and interface layer engineering on the conductivity of ultrathin Ag films. The deposition of indium on the Si(111)7×7 surface at elevated temperatures leads to the formation of a one-dimensional (1D) surface superstructure, consisting of a periodic array of In atomic wires [7]. This Si(111)4×1-In substrate acts as a template for the epitaxial growth of ultrathin Ag(111) films. Scanning tunneling microscopy (STM) shows that the Ag film surface is characterized by a stripe pattern, originating from stacking-fault planes parallel to the In wires, with the same 4× periodicity of the substrate [8]. Angle-resolved photoemission spectroscopy (ARPES) measurements reveal that the films have a quasi-1D quantum well electronic structure, in agreement with the results of the morphological analysis [9]. These experimental findings stimulate electronic transport measurements in order to identify the effects of the substrate-induced structural anisotropy on the electrical conduction of the Ag films.

We performed conductivity measurements by the microscopic four-point probe (4PP) method [10]. The ratio between the sheet conductivity measured along and perpendicular to the 1D structural modulation of the Ag films on Si(111)4×1-In is 1.4 for the 3 ML (monolayer, 1 ML = 2.36 Å) film and reduces with increasing film thickness. Our results clarify that the large anisotropy in the electrical conductivity can be ascribed only partially to the quasi-1D film electronic structure. Instead, a major role in the definition of the transport properties of the Ag films is played by the anisotropic carrier scattering at the film boundaries.

In previous works, anisotropic thin films are realized by using natively anisotropic substrates [11,12] or special techniques [13,14]. Here we suggest that the introduction of a self-assembled single atomic layer at the interface results in a drastic change of the whole thin film transport behavior.

Electric conductivity data were acquired with the independently driven four-tip STM system [15] operated under ultrahigh vacuum condition between 40 and 300 K. The 4PP measurements were carried out in a square geometry [Fig. 1(a)] with a probe spacing of several tens of μm (square-4PP method [10]). Ultrathin Ag(111) films were grown by Ag deposition onto the Si(111)4×1-In or Si(111)7×7 surfaces in the two-step procedure [16]. We define x and y as the directions perpendicular and parallel to the In atomic wires (or $[\bar{1}\bar{1}2]$ and $[1\bar{1}0]$ surface axes, respectively). The ARPES measurements were performed on the VUV-Photoemission beamline (Elettra, Italy) and BL-18A (Photon Factory, KEK, Japan) beamlines.

Figure 1 shows a series of current-voltage curves measured at room temperature (RT) for Ag films grown on different substrates. The experimental geometry is schematically illustrated in Fig. 1(a). The voltage drop between two adjacent probes is measured with a current flow between the other two probes. The values of the resistance along the x and y directions are given by $R_x = V_{12}/I_{43}$ and $R_y = V_{14}/I_{23}$. For the 6 ML Ag

*Present address: Institute of Multidisciplinary Research for Advanced Materials, Tohoku University, 2-1-1 Katahira, Aoba-ku, Sendai 980-8577, Japan; nagamura@tagen.tohoku.ac.jp

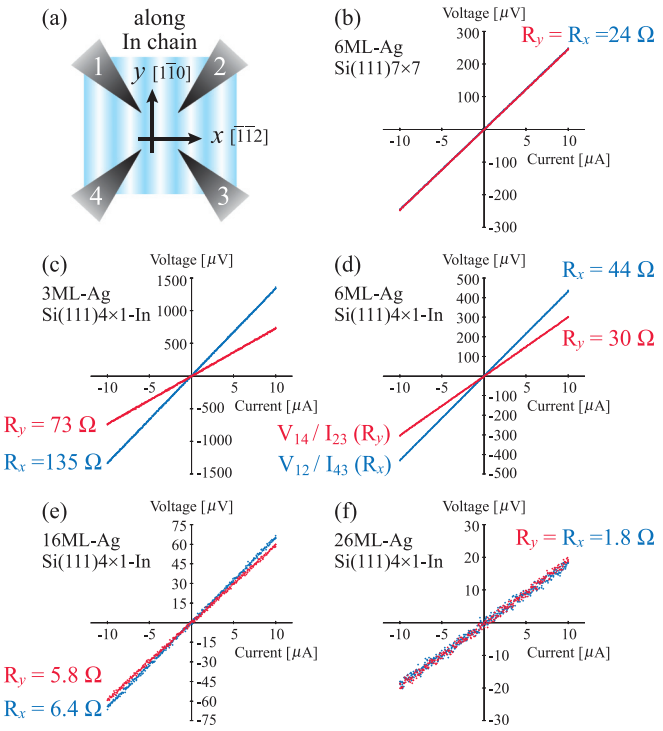

FIG. 1. (Color online) (a) Measurement geometry of the square-4PP method. (b) Current-voltage curves of 6 ML thick Ag(111) films grown on Si(111)7×7. (c)–(f) Those of (c) 3 ML, (d) 6 ML, (e) 16 ML, and (f) 26 ML thick Ag films grown on Si(111)4×1-In. Blue and red data were taken with probe configurations V_{12}/I_{43} and V_{14}/I_{23}, respectively.

film on Si(111)7×7 [Fig. 1(b)] the transport behavior is fully isotropic, thus showing that the use of a stepped substrate influences marginally the film properties [17]. Instead, the R_x and R_y values clearly differ for the 3, 6, and 16 ML Ag films grown on Si(111)4×1-In [Figs. 1(c)–1(e)]. This anisotropy disappears by increasing the Ag thickness to 26 ML [Fig. 1(f)].

The two-dimensional (2D) sheet conductivities of the Ag films, σ_x and σ_y, can be derived from the measured R_x and R_y values by means of the following formulas [10,18]:

$$R_x = \ln(1+\sigma_y/\sigma_x)/2\pi\sqrt{\sigma_x\sigma_y}\,,$$
$$R_y = \ln(1+\sigma_x/\sigma_y)/2\pi\sqrt{\sigma_x\sigma_y}\,.$$

Figure 2(a) shows the σ_x and σ_y values for Ag films of different thickness on the Si(111)7×7 and Si(111)4×1-In substrates. The 2D conductivity (σ) [19], estimated from the bulk Ag crystal properties, is also shown as a black continuous line that drops as the film thickness is reduced. For every investigated coverage, the experimental conductivity values are much smaller than the corresponding bulk-derived values. This difference is derived from the effect of film boundaries which yield surface scatterings and confine electrons in the film [20]. "0 ML" thickness refers to the bare Si(111)4×1-In surface, which is known to display an anisotropic 2D conductivity [10,21]. As expected from Fig. 1, σ_x and σ_y differ markedly for the thinnest Ag films on the Si(111)4×1-In substrate and become similar above 9 ML [22].

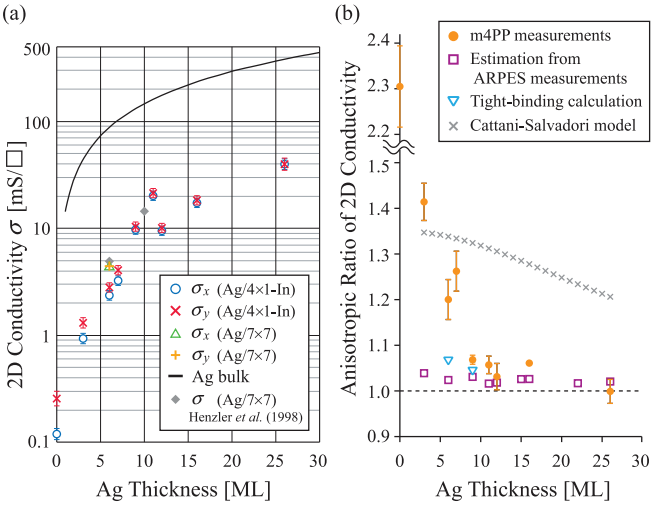

FIG. 2. (Color online) (a) σ_x and σ_y 2D conductivity values for Ag films of different thickness on the Si(111)4×1-In and Si(111)7×7 substrates. The 2D conductivity values σ, estimated from the bulk Ag crystal (black continuous line) or measured by the van der Pawl method [23], are shown for comparison. (b) Ag thickness dependence of the anisotropic ration σ_y/σ_x. Values estimated from different models are also indicated.

The anisotropic character of the electronic transport properties is emphasized in Fig. 2(b), which shows the ratio of the 2D sheet conductivities (σ_y/σ_x). The ratio is ∼2.3 for the Si(111)4×1-In system, in agreement with previous result [21]. σ_y/σ_x amounts to ∼1.4 for the 3 ML Ag film, decreases with increasing film thickness, and becomes 1 at 26 ML Ag.

In order to identify the origin of the observed anisotropy we perform an analysis of the data reported in Fig. 2(b) based on the Boltzmann transport model. The 2D conductivity of a film is given by the following integral equation [24] ($\sigma_x = \sigma_{xx}$ and $\sigma_y = \sigma_{yy}$):

$$\sigma_{ij} = \frac{e^2}{2\pi^2\hbar}\int dk_F \frac{v_{ki}\,v_{kj}\,\tau_k}{|v_k|}\,, \qquad (1)$$

where k_F and v_{ki} ($=\nabla_k E_k/\hbar$) are the Fermi wave vector and the Fermi velocity along the i direction, respectively, while τ_k is the wave-vector-dependent relaxation time. The integral is carried out over the entire Fermi surface. Possible sources of anisotropy in Eq. (1) are the electronic band structure (through k_F and v_{ki}) or the carrier scattering process (through τ_k). The weight of these two factors on the experimental data set can be examined individually.

As an example, the procedure used to estimate σ_x and σ_y for the 6 ML Ag film on Si(111)4×1-In is presented here. Initially, we assume that the relaxation time in Eq. (1) does not depend on the wave vector ($\tau_k = \tau$) and focus on the effects of an anisotropic film electronic structure. The gray-scale ARPES maps for the 6 ML Ag film reported in Figs. 3(a) and 3(b) highlight different band dispersions along the symmetry axes of the system, in analogy with previous findings [9,25]. In the direction parallel to the In atomic wires (k_y) the *sp* quantum well states can be described as parabolas [Fig. 3(b)], interrupted by the interaction with the topmost Si band edges [26]. Along the perpendicular direction (k_x) the

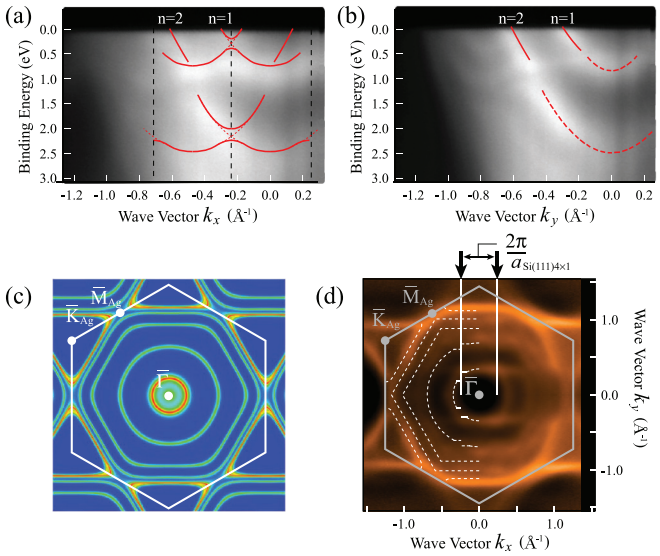

FIG. 3. (Color online) Gray-scale band mapping and Fermi surface of the 6 ML thick Ag films. (a), (b) Gray-scale E_B-$k_{x,y}$ diagram for the Ag film on Si(111)4×1-In along the (a) [$\bar{1}\bar{1}2$] (⊥ In chain) axes and (b) [$1\bar{1}0$] (∥ In chain) axes. Calculated band structures at near the Fermi level are described as solid curves. (c) Fermi surfaces of the freestanding Ag(111) calculated by the tight-binding model. (d) In-plane photoemission intensity map at the Fermi level for the 6 ML thick Ag film on Si(111)4×1-In [29]. The left half of the simplified model for the experimental Fermi surface is drawn by dashed lines on the intensity map. The Ag(111)1×1 surface Brillouin zone and the Si(111)4×1 zone boundary are shown in the figure.

same quantized states appear to be highly distorted near the surface Brillouin zone boundaries [Fig. 3(a)]. Yet, the effective mass (m^*) of these bands at the Fermi level, which determines the Fermi velocity, is almost equal along the two directions. In particular, our data compare well with the results of ARPES measurements for Ag films on Si(111) [9,27] and nearly free electron like model calculations [28], which give $m_x^* = m_y^* = (0.42 \pm 0.06)m_e$, $v_{kx} = v_{ky} = (7.6 \pm 0.23) \times 10^5$ m/s for the $n = 1$ state, and $m_x^* = m_y^* = (0.69 \pm 0.04)m_e$, $v_{kx} = v_{ky} = (9.6 \pm 0.23) \times 10^5$ m/s for $n = 2$–5 states. Here m_e is the rest mass of a free electron and n is the quantum number identifying a quantum well band.

The anisotropic electronic structure of the Ag films emerges more clearly by comparing simulated and measured Fermi surfaces [30]. Figure 3(c) presents tight-binding calculations for the Fermi surface of a freestanding 6 ML Ag(111) film [31]. The energy contours of the quantum well are almost perfectly circular near the $\bar{\Gamma}$ point. At larger in-plane wave vectors, they have a hexagonal-like aspect with corners lying on the $\bar{\Gamma}$-$\bar{M}$ axes because of the gap opening at the $\bar{M}$ point [26]. The photoemission intensity map measured at the Fermi level for the 6 ML Ag film on Si(111)4×1-In [Fig. 3(d)] differs markedly from Fig. 3(c) [29]. The quantum well contours near the zone center appear to be elongated along the k_x axis. Dashed curves in Fig. 3(d) indicate the calculated Fermi surfaces within a 1D nearly free electron band model that takes into account the phase shift and the structure plot [9,32]. This simple model calculation reproduces the ARPES results in the case of a 6 ML Ag(111) film on Si(111)4×1-In, although the energy contours $n = 3$–5 are indistinguishable in the photoemission intensity map. The 2D film conductivity of each quantized state is evaluated from Eq. (1) by substituting experimental parameters (v_{kx}, v_{ky}) mentioned above.

Figure 2(b) reports the anisotropic ratio of the 2D conductivity for each thickness calculated using the procedure reported above for the 6 ML Ag film on Si(111)4×1-In (closed yellowish circles). The σ_y/σ_x values for freestanding films, estimated from tight-binding calculation, are also indicated [open triangles in Fig. 2(b)]. The film electronic structure contribution to the anisotropic ratio is 1.04 at most and appears to have only slight thickness dependence. Especially in the 3–7 Ag ML region the estimated σ_y/σ_x values are much smaller than the experimental ones.

In the second step of our analysis, we evaluate the effects of an anisotropic carrier scattering or wave-vector-dependent τ_k. In a thin-film system with a thickness smaller than or comparable to the carrier mean-free path, the surface and interface are the dominant sources of scattering [33]. Within the Cattani and Salvadori model (C-S model), which takes into account the effect of the surface/interface roughness, the 2D electrical resistivity of a free-electron-like thin film is given by Ref. [11]:

$$\rho_i^{2D} = \frac{\rho_i^{3D}(d)}{d} = \frac{\rho_{bulk}^{3D}}{d}\left[1 + \frac{4 \times 3^{1/3}\pi^{5/3} n_e^{1/3} \hbar \Delta_i^2 \xi_i^2}{\rho_{bulk}^{3D} e^2 d^2 [1 - 6/d(3n_e\pi^5)^{1/3}]}\right], \quad (2)$$

where $\rho_i = 1/\sigma_i$ $(i = x, y)$. ρ_{bulk}^{3D} is the bulk resistivity, n_e the number of free electrons per unit volume, and d the film thickness. The thickness corrugation, Δ_i, and the correlation distance, ξ_i, in the i direction, are adjustable parameters.

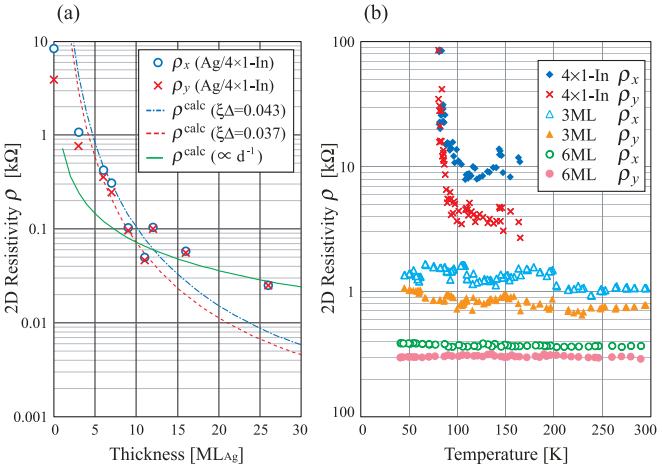

FIG. 4. (Color online) (a) The relation between the film thickness and the 2D resistivity of Ag/Si(111)4×1-In. Calculations by C-S formalism are added by a blue dashed curve and a red dotted curve. A green solid curve represents the function of d^{-1} adjusted to match with the experimental points of the thick films. (b) Temperature dependence of the 2D resistivity of Ag/Si(111)4×1-In at "0 ML" [Si(111)4×1-In bare substrate], 3 ML, and 6 ML of Ag films.

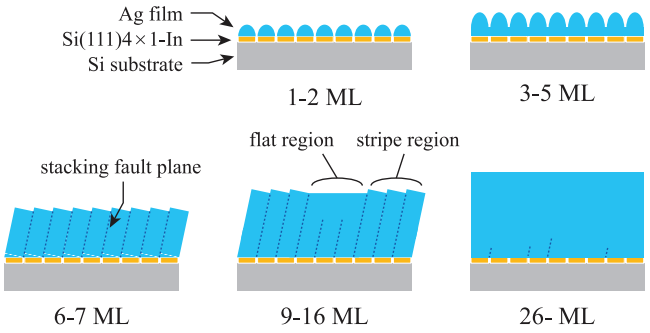

FIG. 5. (Color online) Schematic image of the film morphology in Ag films prepared on Si(111)4×1-In. The upper critical thickness of Ag/Si(111)4×1-In is 3 ML at which percolated highly anisotropic islands are formed without stacking fault planes. The stripe structure based on the stacking-fault model appears at 6 ML. The initial stage of film growth mentioned above is reported in Ref. [8]. The thickness dependence of film morphology at more than 6 ML is estimated from the results of film conductivity shown in Fig. 4(a).

Figure 4(a) reports the experimental resistivity values for the Ag films on Si(111)4×1-In as a function of the film thickness. These data are fitted using Eq. (2) and the Ag bulk values $n_e = 5.85 \times 10^{28}$ m^{-3} and $\rho^{3D}_{bulk} = 1.61 \times 10^{-8}$ Ωm [34]. Within the thickness range 3–9 ML, the experimental results are reproduced reasonably well with $\Delta_y\xi_y = 0.037$ nm^2 (red dashed line) and $\Delta_x\xi_x = 0.043$ nm^2 (blue dash-dotted line). These results are consistent with the STM observation of a larger surface corrugation ($\sim 0.008 \pm 0.003$ nm) along the x direction than along the y direction, whose origin is explained by the stacking-fault structural model [8]. Notably, the difference $\Delta_x\xi_x - \Delta_y\xi_y \sim 0.043$–$0.037 = 0.006$ nm^2 is reproduced if one assumes $\sim$1 nm for the correlation distance of the two directions, that is consistent with the period of a stripe pattern [35].

For larger film thickness the scenario is different. The green continuous line in Fig. 4(a) emphasizes a d^{-1} decrease of the resistivity above 11 ML, which is not reproduced by Eq. (2). The discrepancy is best visualized in Fig. 2(b), where gray crosses indicate the anisotropic ratio estimated from the C-S model ($\sigma_x/\sigma_y = \rho_y/\rho_x$). The magnitude of the anisotropy ratio of the 2D conductivity for the experimental data and the C-S model compare well for the thinnest Ag layers, but differ sizably at higher Ag coverages. The observed behavior could be interpreted in terms of a diminished effect of the anisotropic surface/interface scattering on film transport properties. The STM analysis reported in Ref. [8] seems to corroborate this conjecture. While the striped surface phase dominates for small Ag thickness, 2D flat films form at larger Ag coverages [8]. In other words, the crossover between the two thickness regimes highlighted in Fig. 2(b) is related to the disappearance of the surface stripes on the Ag film as shown in Fig. 5, which describes the thickness dependence of the film morphology. In the 9–16 Ag ML range, where the σ_x/σ_y ratio is very small and almost constant, this could reflect the contribution of the quasi-1D Fermi surface to the anisotropic transport properties of Ag films on Si(111)4×1-In caused by the stacking fault planes remaining in the film at the vicinity of a film/substrate interface.

The carrier scattering at the surface/interface affects the temperature dependence of the film resistivity. Figure 4(b) reports the temperature dependence of the 2D resistivity at "0", 3, and 6 ML Ag films on Si(111)4×1-In. For both 3 and 6 ML thick films ρ changes scarcely over a wide temperature range, but increases drastically for the Si(111)4×1-In substrate below $\sim$100 K, in correspondence with a metal-insulator transition [36–38]. In addition, for the 3 and 6 ML Ag films ρ is one or two orders of magnitude smaller than for the bare Si(111)4×1-In surface. The completely different behavior of the temperature dependence between in Si(111)4×1-In ("0 ML") and in Ag films on Si(111)4×1-In (3, 6 ML) indicate that the contribution from the substrate, Si(111)4×1-In, is negligible. Moreover, the interface scatterings, but not the phonon scatterings, are considered to play a main role in the measured resistivity of Ag films on the Si(111)4×1-In according to showing almost constant resistivity with changing temperature unlike typical bulk metals. These results support our analysis that the surface/interface roughness dominates the resistance and its anisotropy in this range of thickness.

In conclusion, we measured the conductivity of Ag nanofilms grown on a 1D substrate superstructure. The observed anisotropy originates mainly from the anisotropic carrier scattering at the surface/interface of the films, rather than from the quasi-1D Fermi surface. The present results demonstrate that the transport properties of ultrathin metal films can be modified by inserting a single atomic layer at one interface, thus suggesting new strategies for the creation of functional nanostructures.

Takashi Uchihashi and Ayumi Harasawa are gratefully acknowledged for valuable comments and discussions. This work has been supported by Grants-In-Aid from the Japan Society for the Promotion of Science.

[1] K. He, T. Hirahara, T. Okuda, S. Hasegawa, A. Kakizaki, and I. Matsuda, Phys. Rev. Lett. **101**, 107604 (2008).
[2] Z. Zhang, Y. Zhang, Q. Fu, H. Zhang, Y. Yao, T. Ma, D. Tan, Q. Xue, and X. Bao, J. Chem. Phys. **129**, 014704 (2008).
[3] J. Li, M. Przybylski, F. Yildiz, X. D. Ma, and Y. Z. Wu, Phys. Rev. Lett. **102**, 207206 (2009).
[4] S. Mathias, A. Ruffing, F. Deicke, M. Wiesenmayer, I. Sakar, G. Bihlmayer, E. V. Chulkov, Yu. M. Koroteev, P. M. Echenique, M. Bauer, and M. Aeschlimann, Phys. Rev. Lett. **104**, 066802 (2010).
[5] S. S. P. Parkin, N. More, and K. P. Roche, Phys. Rev. Lett. **64**, 2304 (1990).
[6] N. J. Speer, S.-J. Tang, T. Miller, and T.-C. Chiang, Science **314**, 804 (2006); S.-J. Tang, L. Basile, T. Miller, and T.-C. Chiang, Phys. Rev. Lett. **93**, 216804 (2004).
[7] M. Kawaji, S. Baba, and A. Kinbara, Appl. Phys. Lett. **34**, 748 (1979).
[8] T. Uchihashi, C. Ohbuchi, S. Tsukamoto, and T. Nakayama, Phys. Rev. Lett. **96**, 136104 (2006).

[9] N. Nagamura, I. Matsuda, N. Miyata, T. Hirahara, S. Hasegawa, and T. Uchihashi, Phys. Rev. Lett. **96**, 256801 (2006).

[10] T. Kanagawa, R. Hobara, I. Matsuda, T. Tanikawa, A. Natori, and S. Hasegawa, Phys. Rev. Lett. **91**, 036805 (2003).

[11] M. Cattani and M. C. Salvadori, Surf. Rev. Lett. **11**, 283 (2004); M. C. Salvadori, M. Cattani, F. S. Teixeira, R. S. Wiederkehr, and I. G. Brown, J. Vac. Sci. Technol. A **25**, 330 (2007).

[12] C. Tegenkamp, Z. Kallassy, H.-L. Günter, V. Zielasek, and H. Pfnür, Eur. Phys. J. B **43**, 557 (2005).

[13] P. Johnsson, S.-I. Aoqui, A. M. Grishin, and M. Munakata, J. Appl. Phys. **93**, 8101 (2003).

[14] D. Chiappe, A. Toma, and F. Buatier de Mongeot, Phys. Rev. B **86**, 045414 (2012).

[15] H. Hobara, N. Nagamura, S. Hasegawa, I. Matsuda, Y. Yamamoto, Y. Miyatake, and T. Nagamura, Rev. Sci. Instrum. **78**, 053705 (2007).

[16] L. Huang, S. J. Chey, and J. H. Weaver, Surf. Sci. **416**, L1101 (1998).

[17] See Supplemental Material at http://link.aps.org/supplemental/10.1103/PhysRevB.89.125415 for detailed information on the sample.

[18] S. Hasegawa, Chinese J. Phys. **45**, 385 (2007).

[19] The 2D conductivity σ meets $\sigma = \sigma_x = \sigma_y$ in isotropic systems.

[20] R. E. Prange and T.-W. Nee, Phys. Rev. **168**, 779 (1968).

[21] T. Uetake, T. Hirahara, Y. Ueda, N. Nagamura, R. Hobara, and S. Hasegawa, Phys. Rev. B **86**, 035325 (2012).

[22] The σ_i $(i = x, y)$ is larger for 11 ML than for 9 and 12 ML. This observation may suggest the existence of bilayer conductivity oscillations, already reported for ultrathin Pb films [39]. Systematic conductivity measurements as a function of the Ag film thickness are necessary to confirm the conjecture.

[23] M. Henzler, T. Lüer, and A. Burdach, Phys. Rev. B **58**, 10046 (1998).

[24] T. Heinzel, *Mesoscopic Electronics in Solid State Nanostructures*, 3rd ed. (Wiley-VCH, New York, 2010).

[25] K. Kobayashi and T. Uchihashi, Phys. Rev. B **81**, 155418 (2010).

[26] P. Moras, D. Topwal, P. M. Sheverdyaeva, L. Ferrari, J. Fujii, G. Bihlmayer, S. Blügel, and C. Carbone, Phys. Rev. B **80**, 205418 (2009).

[27] M. A. Mueller, T. Miller, and T.-C. Chiang, Phys. Rev. B **41**, 5214 (1990).

[28] N. Miyata, H. Narita, M. Ogawa, A. Harasawa, R. Hobara, T. Hirahara, P. Moras, D. Topwal, C. Carbone, S. Hasegawa, and I. Matsuda, Phys. Rev. B **83**, 195305 (2011).

[29] M. Ogawa, A. Gray, P. M. Sheverdyaeva, P. Moras, H. Hong, L.-C. Huang, S.-J. Tang, K. Kobayashi, C. Carbone, T.-C. Chiang, and I. Matsuda, Phys. Rev. Lett. **109**, 026802 (2012).

[30] As shown in Fig. 3, the Si(111)4×1-In affects the electronic states of Ag quantized states. An anisotropic distortion of Fermi surfaces has been clearly observed in ARPES measurements, while anisotropic m^* at the Fermi level (Fermi velocity) cannot be detected because the difference between m_x^* and m_y^* is small compared to the APPES energy resolution. Therefore, we confine the anisotropy of electronic states only to the shape of Fermi surfaces with the isotropic m^* as a very simple estimation.

[31] We determine the tight-binding parameters to reproduce the band structure of bulk Ag obtained by the density functional calculations and then correct with fixing the parameters related to d orbitals.

[32] I. Matsuda, H. W. Yeom, T. Tanikawa, K. Tono, T. Nagao, S. Hasegawa, and T. Ohta, Phys. Rev. B **63**, 125325 (2001).

[33] T. Hirahara, I. Matsuda, S. Yamazaki, N. Miyata, and S. Hasegawa, Appl. Phys. Lett. **91**, 202106 (2007).

[34] C. Kittel, *Introduction to Solid State Physics*, 8th ed. (Wiley, New York, 2004).

[35] As mentioned in the text, the root mean square of the height of stripe structures which corresponds to the difference of Δ between x and y directions is $\sim$0.008±0.003 nm, and the correlation length ξ which can be considered to be the stripe periodicity is 1.33 nm from the height profiles in the STM observation. This indicates that the difference between $\xi_x \Delta_x$ and $\xi_y \Delta_y$ is estimated as $(0.008 \pm 0.003) \times 1.33 = 0.01 \pm 0.004$ nm^2, which is consistent with our estimation. The root-mean-square roughness, which is a kind of average value, does not represent the height of steps in the stripe structures reported in Ref. [8] as 0.02–0.05 nm.

[36] T. Tanikawa, I. Matsuda, T. Kanagawa, and S. Hasegawa, Phys. Rev. Lett. **93**, 016801 (2004).

[37] J. R. Ahn, J. H. Byun, J. K. Kim, and H. W. Yeom, Phys. Rev. B **75**, 033313 (2007).

[38] Y. J. Sun, S. Agario, S. Souma, K. Sugawara, Y. Tago, T. Sato, and T. Takahashi, Phys. Rev. B **77**, 125115 (2008).

[39] M. Jałochowski and E. Bauer, Phys. Rev. B **38**, 5272 (1988).